

# ESPARGOS: An Ultra Low-Cost, Realtime-Capable Multi-Antenna WiFi Channel Sounder

Florian Euchner, Tim Schneider, Marc Gauger, Stephan ten Brink

Institute of Telecommunications, Pfaffenwaldring 47, University of Stuttgart, 70569 Stuttgart, Germany  
{euchner,gauger,tenbrink}@inue.uni-stuttgart.de

*Abstract*—Multi-antenna channel sounding is a technique for measuring the propagation characteristics of electromagnetic waves that is commonly employed for parameterizing channel models. Channel sounders are usually custom-built from many Software Defined Radio receivers, making them expensive to procure and difficult to operate, which constrains the set of users to a few specialized scientific institutions and industrial research laboratories. Recent developments in Joint Communications and Sensing (JCaS) extend the possible uses of channel data to applications like human activity recognition, human presence detection, user localization and wireless Channel Charting, all of which are of great interest to security researchers, experts in industrial automation and others. However, due to a lack of affordable, easy-to-use and commercially available multi-antenna channel sounders, those scientific communities can be hindered by their lack of access to wireless channel measurements. To lower the barrier to entry for channel sounding, we develop an ultra low-cost measurement hardware platform based on mass-produced WiFi chips, which is easily affordable to research groups and even hobbyists.

## I. INTRODUCTION

Spatial diversity is a crucial concept in modern wireless communication systems enabling improvements in spectral efficiency. Massive multiple-input multiple-output (MIMO) base stations, which exploit this concept, need to continuously estimate the wireless channel to be able to communicate with user equipment (UE) devices, generating large amounts of so-called channel state information (CSI) as a byproduct. Instead of discarding CSI after a successful communication sequence, it can also be exploited by various sensing methods summarized under the umbrella term Joint Communication and Sensing (JCaS). While the idea of JCaS is not new [1], better spatial diversity as well as increasing spectral bandwidths are enabling additional sensing applications which rely on high-dimensional CSI such as Wireless Channel Charting [2].

To better understand performance characteristics of massive MIMO systems and to develop JCaS algorithms, several universities and research laboratories are operating so-called channel sounders, i.e., devices specifically built for CSI measurements. Typically, those channel sounders use protocols and waveforms specifically designed to accommodate for channel estimation. While the acquired channel data is invaluable to progress in the field of

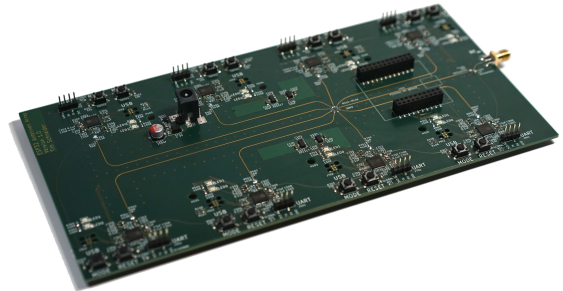


Fig. 1: Picture of prototype circuit board for ESPARGOS

wireless communication systems, channel sounders are usually not suitable for use outside of this field of research: They require qualified operators, are expensive and difficult to set up and may even involve obtaining frequency allocations or an amateur radio license.

Due to these downsides, researchers in other domains who work with wireless channel data have often turned to WiFi: Often-quoted WiFi sensing applications include human presence and activity detection, traffic monitoring, gesture and sign language recognition, localization, imaging and others [3], with many privacy-sensitive applications such as gesture / pose detection [4] [5] also sparking interest and concerns among the general public. Common methods for WiFi CSI acquisition are the use of software-defined radios (SDRs), software libraries for Intel and Atheros WiFi cards [6] [7] as well as software libraries for extracting CSI from WiFi-capable Espressif ESP32 microcontrollers [8] [9]. The major disadvantage of these inexpensive channel sounding techniques is the low number of MIMO channels, usually only three antennas or even fewer, which is unfavorable for sensing applications that greatly benefit from spatial diversity. Simply using multiple WiFi cards or microcontrollers without taking additional precautions does not produce phase-coherent CSI due to lack of synchronization – data acquired this way would be unusable for many JCaS algorithms, including e.g. angle of arrival (AoA) estimation. Proposed workarounds like antenna switching [10] come with their own downsides, such as requiring multiple frame transmissions for one sensing operation.

To overcome these challenges, we propose ESPARGOS (a portmanteau of ESP32 and Argos Panoptes, the greek

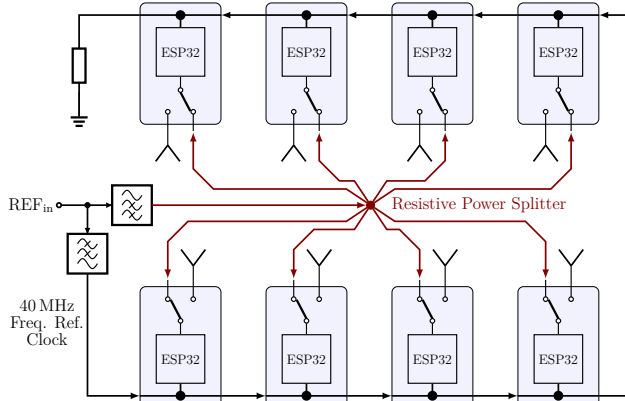


Fig. 2: Block diagram showing all components related to synchronization on an ESPARGOS circuit board, with the distribution network for the phase reference signal in red.

mythological many-eyed giant), a low-cost, single-circuit board (see Fig. 1) approach to a coherent and easy-to-operate many-antenna WiFi channel sounder, geared towards prototyping WiFi sensing devices.

The remainder of this paper is structured as follows: The hardware and software architecture of ESPARGOS are explained in Section II and III, respectively. Characterizations and measurement results are presented in Section IV and Section V summarizes our work and provides an outlook.

## II. HARDWARE ARCHITECTURE

Inspired by KrakenSDR [11], ESPARGOS is made up of several ESP32 microcontrollers, operated in receive-only mode. All hardware components, including eight ceramic antennas, are mounted on a single four-layer FR4 circuit board, making ESPARGOS inexpensive and easy to produce and deploy. A pin header on the circuit board exposes a Serial Peripheral Interface (SPI) bus, which can be used to interface the board with a computer. As illustrated in Fig. 2, all microcontrollers are clocked by a daisy-chained 40 MHz reference oscillator, ensuring frequency synchronization.

### A. Source of Phase Uncertainty

Reference clock distribution is insufficient for achieving phase coherence: While the internal structure of the ESP32 chip is not publicly known, it is reasonable to assume that the local oscillator (LO) signal is generated from the reference clock using a PLL (see Fig. 3), which may exhibit phase uncertainty between reference clock and output clock. This phase uncertainty is a common property of PLLs and can have multiple sources, including ambiguities in the phase detector, unknown initial digital counter states in the forward “ $1/r$ ” frequency divider (see Fig. 4) and voltage controlled oscillator (VCO) center frequency inaccuracies [12] [13]. By measurement it was determined that, indeed, the initial phase changes after a chip reset and after modifying the LO frequency (WiFi channel), likely every time the PLL has to acquire a

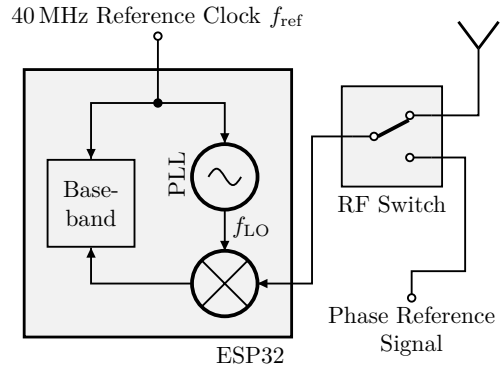


Fig. 3: Block diagram of a single receiver: The ESP32 is frequency-synchronized using both a 40 MHz reference clock and, to ensure coherence, a WiFi-based phase reference signal

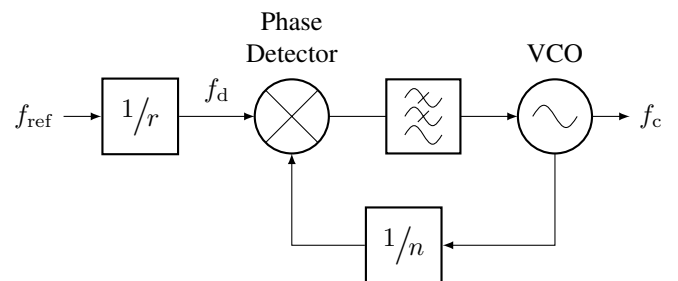


Fig. 4: Block diagram of a typical integer- $n$  phase-locked loop. The phase locked loop (PLL) in the ESP32 may be implemented in a similar fashion, synthesizing carrier frequency  $f_c$  from reference clock  $f_{ref}$ .

new frequency lock. Furthermore, even if this source of ambiguity did not exist, analog components may introduce receiver-specific phase shifts due to e.g. process variation or temperature dependencies. Hence, an additional, periodically performed phase calibration step is vital to ensure phase coherence.

### B. Phase Reference Signal Distribution

In the case of ESPARGOS, as shown in Fig. 2 and Fig. 3, each ESP32 is connected to an RF switch that can alternate between the ceramic antenna and a WiFi-based phase reference signal provided to every receiver using a distribution network made up of a resistive divider and microstrip transmission lines. The phase reference signal generator must simply produce valid WiFi frames, which can be received by the ESP32 chip. Since the expected phase differences between any two receivers are known for the reference signal (they are determined by the geometry of the distribution network), receiver-specific phase offsets can be calibrated for.

By feeding reference clock and phase calibration signal from external sources, multiple circuit boards can be combined into one large phase-coherent system. To reduce the amount of cabling required, the 40 MHz reference

clock and the WiFi-based phase reference signal are fed via the same coaxial cable and separated on the circuit board using appropriate high-pass and low-pass filters (see Fig. 2).

### III. SOFTWARE

The ESP32's WiFi driver provides CSI estimated from the Legacy Long Training Field (LLTF) [14, Section 20.3.9.3.4] and High Throughput Long Training Field (HTLTF) [14, Section 20.3.9.4.6], which are a part of received WiFi frames, through a software interface. In a so-called promiscuous mode, this CSI acquisition can be carried out passively, i.e., the receivers can sniff WiFi frames without transmitting anything themselves. The raw CSI data is then transferred to a central computer through the SPI bus, where CSI from all receivers is combined and analyzed.

#### A. CSI Acquisition

Since the WiFi frames are received by the ESP32 microcontrollers independently from one another, they must first be clustered. Received frames that correspond to the same transmitted frame can be identified based on MAC address, receiver timestamp (thanks to synchronized sampling clocks) and packet headers. For each time index  $t$ , the matrix of true (physical) subcarrier channel coefficients is denoted by

$$\mathbf{H}[t] = \left( \mathbf{h}^{(1)}[t], \dots, \mathbf{h}^{(N)}[t] \right) \in \mathbb{C}^{M \times N},$$

where  $M$  is the number of receive antennas and  $N$  the number of usable orthogonal frequency division multiplex (OFDM) subcarriers.

In practice,  $\mathbf{H}[t]$  cannot be measured directly, but the reported channel coefficients  $r_m^{(n)}[t]$  are noisy due to estimation and quantization errors. Despite these shortcomings, by assuming CSI stationarity over short time intervals, the goal of obtaining good estimates  $\hat{\mathbf{H}} = (\hat{\mathbf{h}}^{(1)}, \dots, \hat{\mathbf{h}}^{(N)})$  of the true CSI matrix is achievable by taking into account several consecutive measurements. For the following derivations, we consider a single subcarrier  $n$  and drop the subcarrier index in our notation, i.e.  $\mathbf{h}[t] = \mathbf{h}^{(n)}[t]$  and  $\mathbf{r}[t] = \mathbf{r}^{(n)}[t]$  for simplicity. However, the approach can be extended to multiple subcarriers by simply applying the same technique to every subcarrier independently.

Let  $\mathcal{R} = \{(t_1, m_1), (t_2, m_2), \dots\}$  denote a set that contains tuples of time and antenna indices of all the channel coefficients measured within the considered interval, where  $r_m[t]$  with  $(t, m) \in \mathcal{R}$  is the channel coefficient for antenna  $m$  measured at time instance  $t$ .  $r_m[t]$  is affected by the initial phase  $\varphi$  of the transmitter, which is different for every time index  $t$  and unknown due to unknown oscillator frequency offset and oscillator drift. As a consequence, all channel coefficients for one particular time instance may be phase-rotated by a common factor  $e^{j\varphi}$ . Furthermore, we assume that  $\mathbf{r} \in \mathbb{C}^M$  is affected by additive i.i.d. noise  $\mathbf{n} \in \mathbb{C}^M$ :

$$\mathbf{r} = \mathbf{h} e^{j\varphi} + \mathbf{n}$$

$\varphi \in [-\pi, \pi)$  and  $\mathbf{n}$  are modelled as independent random variables. While the distribution for  $\varphi$  is unknown, we assume that  $\mathbf{n}$  is zero-mean with  $\mathbb{E}[\mathbf{n}\mathbf{n}^H] = \sigma^2\mathbf{I}$ .

Instead of estimating  $\mathbf{h}$  directly from multiple measurements of  $\mathbf{r}$ , we first compute the covariance matrix  $\mathbf{C}$  of  $\mathbf{r}$  as

$$\mathbf{C} = \mathbb{E}[\mathbf{r}\mathbf{r}^H] = \mathbf{h}\mathbf{h}^H + \sigma^2\mathbf{I}.$$

In practice, we can only estimate the sample covariance matrix  $\hat{\mathbf{C}}$  from the finite number of samples  $\mathbf{r}[t] = (r_1[t], \dots, r_M[t])^T$ ,  $t = 1 \dots T$  measured within the considered interval:

$$\hat{\mathbf{C}} = \frac{1}{T} \sum_{t=1}^T \mathbf{r}[t]\mathbf{r}[t]^H \quad (1)$$

In many cases, one or more of the receivers may miss a WiFi frame and therefore not provide CSI for any particular WiFi frame, which makes (1) unsuitable. The underlying reasons for this loss of frames are unknown and hard to analyze without knowledge about the inner workings of the ESP32 chip. Instead of requiring data from all  $M$  antennas as in (1), we can also estimate  $\mathbf{C}$  from incomplete CSI vectors: Let  $\mathcal{T}_{ij} = \{t \mid (t, i) \in \mathcal{R}, (t, j) \in \mathcal{R}\}$  denote the set of time indices for which channel coefficients are available from both antenna  $i$  and  $j$ . We obtain the sample covariance matrix  $\hat{\mathbf{C}}$  by estimating the individual entries of the matrix as follows:

$$\hat{C}_{ij} = \frac{1}{|\mathcal{T}_{ij}|} \sum_{t \in \mathcal{T}_{ij}} r_i[t]r_j[t]^*$$

Due to the limited number of samples,  $\hat{\mathbf{C}}$  is only a noisy estimate of  $\mathbf{C}$ , with noise matrix  $\mathbf{Z}$  modelled as a zero-mean random variable:

$$\hat{\mathbf{C}} = \mathbf{C} + \mathbf{Z} = \mathbf{h}\mathbf{h}^H + \sigma^2\mathbf{I} + \mathbf{Z} \quad (2)$$

Since the distribution of  $\mathbf{Z}$  is unknown, we propose to solve (2) for  $\mathbf{h}\mathbf{h}^H$  using a least-squares approach, where we minimize  $\mathbf{Z}$  w.r.t. the Frobenius norm:

$$\begin{aligned} \hat{\mathbf{h}} &= \arg \min_{\boldsymbol{\vartheta} \in \mathbb{C}^M} \left\| (\hat{\mathbf{C}} - \sigma^2\mathbf{I}) - \boldsymbol{\vartheta}\boldsymbol{\vartheta}^H \right\|_F^2 \\ &= \arg \max_{\boldsymbol{\vartheta} \in \mathbb{C}^M} 2\boldsymbol{\vartheta}^H(\hat{\mathbf{C}} - \sigma^2\mathbf{I})\boldsymbol{\vartheta} - \|\boldsymbol{\vartheta}\|^4 \end{aligned} \quad (3)$$

By setting the derivative w.r.t.  $\boldsymbol{\vartheta}$  to  $\mathbf{0}$ , we obtain

$$\begin{aligned} (\hat{\mathbf{C}} - \sigma^2\mathbf{I})\boldsymbol{\vartheta} &= \|\boldsymbol{\vartheta}\|^2\boldsymbol{\vartheta} \\ \hat{\mathbf{C}}\boldsymbol{\vartheta} &= (\|\boldsymbol{\vartheta}\|^2 + \sigma^2)\boldsymbol{\vartheta} \end{aligned} \quad (4)$$

which is a necessary condition for an optimum. Clearly, (4) is fulfilled by all vectors  $\boldsymbol{\vartheta}$  that are appropriately scaled eigenvectors of  $\hat{\mathbf{C}}$ . Namely, they need to be scaled according to their corresponding eigenvalue  $\lambda \geq 0$  (since  $\hat{\mathbf{C}}$  is positive semidefinite), such that  $\|\boldsymbol{\vartheta}\| = \sqrt{\lambda - \sigma^2}$ . From (3) we see that the objective function is maximized if the eigenvector  $\boldsymbol{\vartheta}$  with the largest corresponding eigenvalue  $\lambda$  is chosen, i.e., the principal eigenvector. Hence, the estimate  $\hat{\mathbf{h}}$  is chosen out of the set  $\{(\boldsymbol{\vartheta}_\ell, \lambda_\ell)\}$  of

eigenvectors with corresponding eigenvalues of  $\hat{\mathbf{C}}$  and scaled accordingly:

$$\ell_{\text{princ}} = \arg \max_{\ell} \{\lambda_{\ell}\} \rightarrow \hat{\mathbf{h}} = \sqrt{\lambda_{\ell_{\text{princ}}} - \sigma^2} \frac{\mathcal{D}_{\ell_{\text{princ}}}}{\|\mathcal{D}_{\ell_{\text{princ}}}\|}$$

### B. Phase and Power Calibration

For phase calibration, we again consider the case of a single subcarrier  $n$  with  $\hat{\mathbf{h}}_{\text{OTA}} = \hat{\mathbf{h}}_{\text{OTA}}^{(n)} \in \mathbb{C}^M$  denoting the estimated channel vector for the over-the-air channel between ESPARGOS antenna array and some WiFi transmitter.

Two types of phase calibrations need to be carried out to achieve phase-coherent receivers:

- Removal of the unknown PLL / analog hardware phase offsets with the help of the phase reference signal and
- calibration for the propagation delays of the phase reference signal passing through the distribution network on the circuit board itself, which manifest themselves in antenna-specific phase offsets  $\varphi_{\text{path},m}$ .

The PLL phase offsets are estimated based on the phase reference signal, resulting in another channel vector estimate  $\hat{\mathbf{h}}_{\text{REF}} \in \mathbb{C}^M$ . The estimation procedures for both the over-the-air channel and for the PLL phase offsets are carried out independently, as explained in Section III-A – the two different channels (over-the-air and reference signal distribution network) can be distinguished either by the state of the RF switch, or, more reliably, by embedding some reference indicator into the WiFi frames of the reference signal. By assuming the difference in attenuation across the individual paths of the reference signal distribution network is negligible, the reference signal amplitudes may also be used for power calibration. Overall, power- and phase-calibrated channel coefficients  $\hat{h}_{\text{CAL},m}$  which account for both PLL / analog hardware phase offsets and reference distribution network phase offsets, can be computed as

$$\hat{h}_{\text{CAL},m} = \frac{\hat{h}_{\text{OTA},m}}{\hat{h}_{\text{REF},m}} e^{-j\varphi_{\text{path},m}}.$$

For a single  $2 \times 4$  ESPARGOS antenna array, the antenna-specific phase offsets due to the distribution network path delays  $\varphi_{\text{path},m}$  are a result of the circuit board layout and are constant. If multiple ESPARGOS antenna arrays are combined, the phase offsets induced by the reference signal distribution network outside of the antenna arrays, typically consisting of power splitters and coaxial cables, also need to be taken into account.

## IV. ANALYSES AND MEASUREMENTS

### A. Phase Stability

For the phase stability experiment, we forgo aforementioned phase and power calibration step and only take into account the over-the-air channel estimates  $\hat{h}_{\text{OTA},m}^{(n)}$ . We

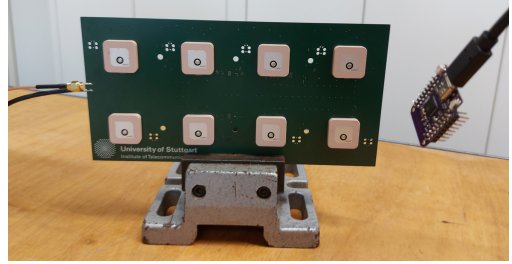


Fig. 5: Experiment setup: Frontal view of ESPARGOS and another ESP32 development board used as transmitter

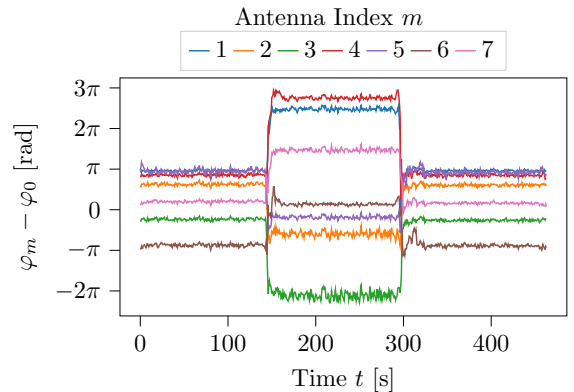


Fig. 6: Phase differences (moving average over 20 samples) between antennas over time: Transmitter is relocated at  $t \approx 150$  s and moved back to its original location at  $t \approx 300$  s.

compute the phase over the sum of the channel coefficients of all  $N$  subcarriers:

$$\varphi_m = \arg \left\{ \sum_{n=1}^N \hat{h}_{\text{OTA},m}^{(n)} \right\}$$

Note that this averaging is only sensible for sufficiently frequency-flat channels such as indoor channels with low delay spread. Long-term phase stability is achieved if, in a static environment, the phase differences  $\varphi_m - \varphi_{m_0}$  between any two antennas  $m, m_0$ ,  $m \neq m_0$  remain constant over long intervals. We typically express all phase differences relative to the same antenna with index  $m_0$  which we call the “reference antenna”.

Synchronizing receivers in frequency using the 40 MHz reference clock signal should be sufficient for achieving long-term phase stability, even if no phase reference signal is provided. To test this assumption, a simple experiment was conceived and carried out. The experiment setup is shown in Fig. 5: The ESPARGOS circuit board is fixated to a stand and another, mobile ESP32 microcontroller is used as a WiFi transmitter. The transmitter is first placed at some marked location, after some time relocated to another place and later moved back to its original location. Fig. 6, which shows the resulting measured phase differences over time with reference antenna  $m_0 = 0$  for a single 20 MHz wide WiFi channel, qualitatively demonstrates that phase stability is the case for ESPARGOS:

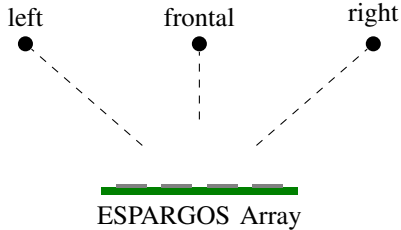


Fig. 7: Illustration of three considered transmitter placements “left”, “frontal” and “right” (not drawn to scale)

Unless the transmitter is moved, the variance in the phase difference between any two of the eight antennas in the array is small.

### B. Angle of Arrival Measurement

In another experiment, the suitability of ESPARGOS for a simple AoA estimation task is examined. Phase and power calibration are applied as previously described and the AoA estimates are computed based on the fully calibrated channel coefficient estimates  $\hat{h}_{\text{CAL},m}$ .

As a proof for the feasibility of the system, we only consider a simple qualitative test, namely whether ESPARGOS can distinguish between three different transmitter placements. In this setup, ESPARGOS is again fixated in a stand as shown in Fig. 5 and channel coefficients for the three transmitter locations illustrated in Fig. 7 are measured. Namely, the transmitter is either located directly in front of the antenna array at a distance of a few meters, or shifted to the right or to the left from the frontal position.

The phases of the estimated channel coefficients  $\hat{h}_{\text{CAL},m}$  for the three different transmitter locations are illustrated in Fig. 8, by coloring antennas according to the received phases in frontal views of the antenna array. Even by just looking at the measured phase patterns, it is easy to see that information about the AoA is contained within  $\hat{h}_{\text{CAL},m}$ : Depending on the transmitter location, the received phases either increase from left to right, from right to left or are approximately the same over all antennas.

For a practical application of ESPARGOS, AoA estimation algorithms such as MUSIC [15] could be applied to the received channel coefficients  $\hat{h}_{\text{CAL},m}$ . As explained in [15], MUSIC computes a spatial pseudo-spectrum by assigning a power value to every potential angle  $\Theta$  of an incident wave. Clearly, the spatial pseudo-spectra obtained for the measurements using the MUSIC algorithm, shown in Fig. 9, easily permit distinguishing between the three different transmitter locations.

## V. CONCLUSION AND OUTLOOK

The concept of a realtime-capable WiFi channel sounder which, despite its very low cost, can achieve a high degree of spatial diversity was presented and a prototype was qualitatively evaluated in a simple practical application. Quantitative performance testing and further

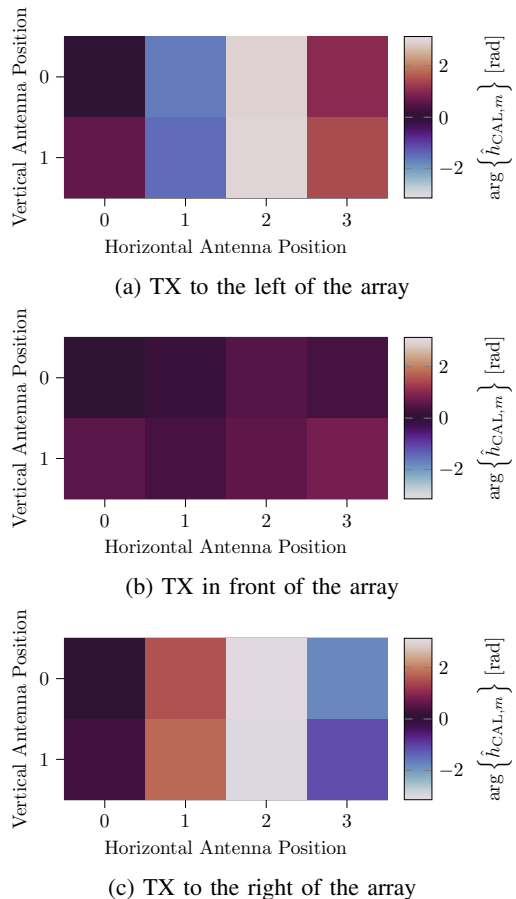
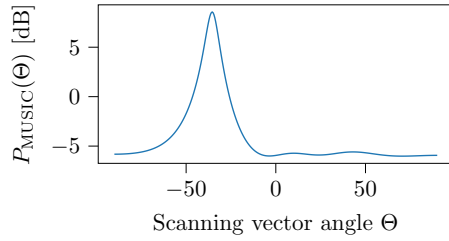


Fig. 8: Received signal phase visualized over antennas, frontal view of ESPARGOS, with transmitter located at different positions relative to the receiver array. For the illustration, the top-left antenna in the array  $m_0 = 0$  (vertical and horizontal index 0) is used as a phase reference (i.e., its phase is always  $\arg\{\hat{h}_{\text{CAL},0}\} = 0$ ).

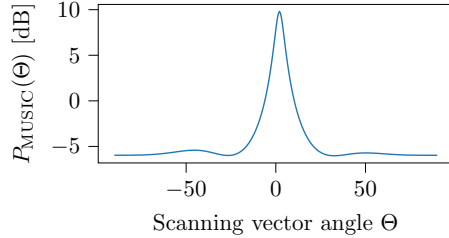
characterizations of the system remain a subject for future study. While ESPARGOS could never replace dedicated multi-antenna channel sounders employed in wireless research, it could be a useful tool for experiments in domains like JCaS and security research if the quality of measurements turns out to be sufficient for such applications. In the future, we plan to apply ESPARGOS to applications like Channel Charting. Furthermore, the basic concepts behind the architecture of ESPARGOS are transferable to similar application-specific channel sounders.

## REFERENCES

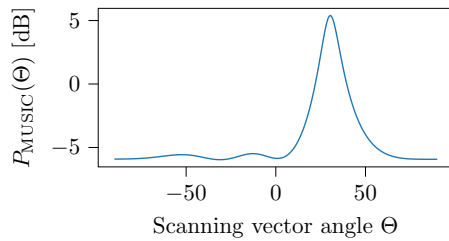
- [1] C. Sturm and W. Wiesbeck, “Waveform design and signal processing aspects for fusion of wireless communications and radar sensing,” *Proceedings of the IEEE*, vol. 99, no. 7, pp. 1236–1259, 2011.
- [2] C. Studer, S. Medjkouh, E. Gönültaş, T. Goldstein, and O. Tirkkonen, “Channel Charting: Locating Users within the Radio Environment using Channel State Information,” *CoRR*, vol. abs/1807.05247, 2018. [Online]. Available: <http://arxiv.org/abs/1807.05247>
- [3] Y. Ma, G. Zhou, and S. Wang, “WiFi Sensing with Channel State Information: A Survey,” *ACM Computing Surveys (CSUR)*, vol. 52, no. 3, pp. 1–36, 2019.



(a) TX to the left of the array



(b) TX in front of the array



(c) TX to the right of the array

Fig. 9: Spatial pseudo-spectra computed with the Multiple Signal Classification (MUSIC) algorithm

- [4] F. Adib and D. Katabi, "See through walls with WiFi!" in *Proceedings of the ACM SIGCOMM 2013 conference on SIGCOMM*, 2013, pp. 75–86.
- [5] J. Geng, D. Huang, and F. De la Torre, "DensePose From WiFi," *arXiv preprint arXiv:2301.00250*, 2022.
- [6] D. Halperin, W. Hu, A. Sheth, and D. Wetherall, "Tool release: Gathering 802.11n traces with channel state information," *ACM SIGCOMM CCR*, vol. 41, no. 1, p. 53, Jan. 2011.
- [7] Y. Xie, Z. Li, and M. Li, "Precise Power Delay Profiling with Commodity WiFi," in *Proceedings of the 21st Annual International Conference on Mobile Computing and Networking*, ser. MobiCom '15. New York, NY, USA: ACM, 2015, p. 53–64. [Online]. Available: <http://doi.acm.org/10.1145/2789168.2790124>
- [8] S. M. Hernandez and E. Bulut, "Lightweight and Standalone IoT Based WiFi Sensing for Active Repositioning and Mobility," in *21st International Symposium on "A World of Wireless, Mobile and Multimedia Networks" (WoWMoM) (WoWMoM 2020)*, Cork, Ireland, June 2020.
- [9] M. Atif, S. Muralidharan, H. Ko, and B. Yoo, "Wi-ESP — A tool for CSI-based Device-Free Wi-Fi Sensing (DFWS)," *Journal of Computational Design and Engineering*, 05 2020, qwaa048. [Online]. Available: <https://doi.org/10.1093/jcde/qwaa048>
- [10] J. C. L. Yaxiong Xie, Yanbo Zhang and M. Li, "SWAN: Stitched Wi-Fi Antennas," in *Proceedings of the 24th Annual International Conference on Mobile Computing and Networking*, ser. MobiCom '18. ACM, 2018.
- [11] KrakenRF Inc, "KrakenSDR - A Coherent Radio Receiver for Radio Direction Finding and Passive Radar." [Online]. Available: <https://www.krakenrf.com/>
- [12] D. R. Brown, G. B. Prince, and J. A. McNeill, "A method for carrier frequency and phase synchronization of two autonomous cooperative transmitters," in *IEEE 6th Workshop on Signal Processing Advances in Wireless Communications, 2005*. IEEE, 2005, pp. 260–264.
- [13] T. Toroni, "Multi-Clock Synchronization," Texas Instruments, Tech. Rep., 2019.

- [14] "IEEE Standard for Information technology – Telecommunications and information exchange between systems Local and metropolitan area networks—Specific requirements Part 11: Wireless LAN Medium Access Control (MAC) and Physical Layer (PHY) Specifications," *IEEE Std 802.11-2012 (Revision of IEEE Std 802.11-2007)*, 2012.
- [15] R. Schmidt, "Multiple emitter location and signal parameter estimation," *IEEE Transactions on Antennas and Propagation*, vol. 34, no. 3, pp. 276–280, 1986.